Experimental Demonstration of a Controllable Electrostatic Molecular Beam Splitter

Lianzhong Deng, Yan Liang, Zhenxing Gu, Shunyong Hou, Shengqiang Li, Yong Xia, and Jianping Yin*

State Key Laboratory of Precision Spectroscopy, Department of physics, East China Normal University, Shanghai 200062, People's Republic of China

(Received 11 May 2010; published 5 April 2011)

We experimentally demonstrate a controllable electrostatic beam splitter for guided ND_3 molecules with a single Y-shaped charged wire and a homogeneous bias field generated by a charged metallic parallel-plate capacitor. We study the dependences of the splitting ratio R of the guided ND_3 beam and its relative guiding efficiency η on the voltage difference between two output arms of the splitter. The influences of the molecular velocity v and the cutting position L on the splitting ratio R are investigated as well, and the guiding and splitting dynamic processes of cold molecules are simulated. Our study shows that the splitting ratio R of our splitter can be conveniently adjusted from 10% to 90% by changing ΔU from -6 kV to $+6$ kV, and the simulated results are consistent with our experimental ones.

DOI: 10.1103/PhysRevLett.106.140401 PACS numbers: 03.75.Be, 37.10.Gh, 37.10.Mn, 37.20.+j

Matter-wave beam splitters are one of the key elements in atom and molecule optics, and have some important applications. The matter-wave beam splitters are mainly classified as free-space beam splitters and waveguide beam splitters. Usually, the atomic- or molecular-beam splitters in free space, such as mechanical grating splitter [1], standing-wave diffraction splitter [2], Bragg diffraction splitter [3], $\pi/2$-pulsed internal-state splitter [4], and so on [5], are a kind of coherent matter-wave beam splitters, which can be used to form various atom or molecule interferometers [6,7], and then to perform precise measurements [8], even to study the coherences of atomic or molecular matter waves [9,10] and basic physics [11], etc. Generally, when the guiding and splitting processes of cold atoms or molecules are multimode and incoherent, the waveguide beam splitters are a kind of incoherent ones, which also have some important applications in atom or molecule optics. For this, various waveguide atomic-beam splitters, such as magnetic-waveguide beam splitters using a Y-shaped current-carrying wire [12], laser-guided beam splitters using two crossing Gaussian beams [13] or two crossing cylindrical microlenses [14], were proposed and demonstrated. More recently, we proposed a simple scheme to split a cold molecular beam by using a single Y-shaped charged wire [15]. However, the feasibility of this beam splitter has not been demonstrated experimentally. Also, to our knowledge, no other waveguide molecular-beam splitter to date has been proposed and studied both theoretically and experimentally.

In this Letter, we experimentally demonstrate the first beam splitter for the guided supersonic ND_3 beams and study the dependences of the splitting ratio R of the guided ND_3 beam and its relative guiding efficiency η on the voltage difference ΔU between two output arms of the Y-shaped wire. The influences of both the molecular longitudinal velocity v and the cutting position L on the splitting ratio R are investigated as well. Three-dimensional Monte Carlo simulations for the processes of guiding and splitting ND_3 molecules are performed.

Our experimental setup for splitting supersonic molecular beams is shown in Fig. 1(a). A pulsed supersonic molecular beam is formed by adiabatically expanding a gaseous mixture of $\sim$5% ND_3 in xenon through a modified solenoid valve (General Valve, Series 99, whose temperature can be changed from 300 to 150 K by cooling liquid nitrogen with a heating controller) with a 0.5 mm

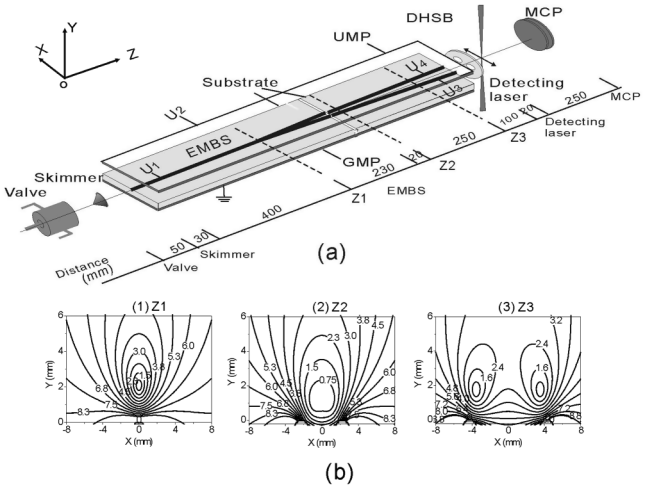

FIG. 1. (a) Experimental setup for splitting a supersonic molecular beam by using a Y wire and the locations of each element with distances between them. EMBS, UMP, GMP, DHSB, and MCP stand for electrostatic molecular-beam splitter, upper metal plate, grounded metal plate, double-hole sampling board, and microchannel plate. (b) Contours of the electric field magnitude in the xy plane at three selected positions $z1$ (1) (the geometric diverging point of the Y wire), $z2$ (2) (250 mm downstream from $z1$), and $z3$ (3) (500 mm downstream from $z1$), respectively, with $U_1 = U_3 = U_4 = 16$ kV and $U_2 = 18$ kV. The electric field magnitude is shown in units of kV/cm.

diameter opening into the source chamber. The operating pressure in the source and working chambers is typically $\sim 2.0 \times 10^{-4}$ Pa and $\sim 2.0 \times 10^{-6}$ Pa, respectively. After passing through a skimmer with a diameter of 1.0 mm, the molecular beam enters a homemade electrostatic molecular-beam splitter (EMBS), situated in the working chamber. The output molecular beams from two sampling holes are detected by using the resonantly enhanced multiphoton ionization spectrum, and the molecular ions are extracted and collected by a dual microchannel-plate (MCP) detector downstream. The two symmetric sampling rectangle holes with an open area of 4 mm × 6 mm are separated by a center-to-center distance of 10 mm. The frequency-doubled dye laser for detection has single-pulse energy of ~10 mJ and is focused (with a focal length of ~300 mm) on the molecules. The laser wavelength is around 317 nm and ND_3 molecules in the weak-field-seeking (WFS) state of $|J = 1, KM = -1\rangle$ are detected.

The structure of the homemade EMBS is described as follows: a Y wire with a diameter of 2 mm is totally embedded in a ceramic substrate ($\varepsilon_r = 6.5$) with a thickness of 14 mm. As shown in Fig. 1(a), the lengths of the straight and branching parts of the Y-shaped wire are 400 and 600 mm, respectively. The input arm of the Y wire is charged by a high voltage U_1 with its two output arms being charged by high voltages U_3 and U_4, respectively. The center-to-center distance of the two output arms at the outlet is 10 mm, corresponding to a diverging angle of ~1.9°. A large parallel stainless-steel plate with the same size as the ceramic substrate is horizontally placed over the Y wire with a distance of 10 mm and charged by a high voltage U_2, whereas another stainless-steel plate is placed under the ceramic substrate and grounded. By selecting appropriate values of U_1, U_2, U_3, and U_4, a Y-shaped hollow electrostatic guiding tube for the WFS ND_3 molecules can be formed above the surface of the Y wire. Figure 1(b) shows the contours of the electric field magnitude in the xy plane at three selected positions $z1$, $z2$, and $z3$, with $U_1 = U_3 = U_4 = 16$ kV and $U_2 = 18$ kV. The distance of the electrostatic guiding center from the substrate surface is about 2 mm. The WFS ND_3 molecules moving inside the Y-shaped hollow electrostatic tube will first experience a transverse electric dipole gradient force towards the central electric field minimum and be guided along the z direction, and then be split into two molecular branches with a 50%-50% splitting ratio after the splitting point. To form a controllable beam splitter, the two output arms of the Y wire are cut off at a position of $L = 230$ mm downstream from the forked point and set apart with a gap of ~1 mm to avoid possible electrical discharges. By changing the voltage difference $\Delta U = U_3 - U_4$ between the two output arms of the Y wire, we can adjust the splitting ratio of our EMBS. In the experiment, the temperature of the pulse valve is set as 220 K, and the longitudinal velocity distribution of the supersonic ND_3 beam is centered around 300 m/s with a velocity spread of about 20%. The transverse velocity distribution is centered around zero with a spread of about 15 m/s in both x and y directions. The pulse valve is operated at a frequency of 10 Hz, and all experimental data are averaged over 128 shots.

We first studied the dependence of the guided molecules in the two output branches on the voltage difference ΔU. When $U_1 = 16$ kV and $U_2 = 18$ kV, we change $\Delta U = U_3 - U_4$ from +6 kV to −6 kV and measure the transverse profiles of the guided molecules at the two outlets of the splitter by scanning the detecting laser transversely. Solid symbols with an error bar in Fig. 2 are the measured ion signals of the transverse profiles of guided molecules for three selected values of $\Delta U = +6$ kV (triangles), 0 kV (circles), and −6 kV (squares), respectively. Open symbols in Fig. 2 represent the ion signals of free-flying molecules without any voltage applied. Figures 2(a) and 2(b) are the experimental and simulated results for the two cases without and with the sampling board, respectively. The sampling board is introduced here to reduce the influences resulting from both the scattering background [see a broad and smooth background distribution in Fig. 2(a)] of the nonguided molecules from the surfaces of the both upper plate and ceramic substrate as well as those directly transmitted fast molecules [see a central "hump" or "hillside" distribution in Fig. 2(a)], so that we can better interpret the transverse profile of the guided molecules. From Fig. 2, we can see that when the voltage difference $\Delta U = 0$ kV, the ion signals of the guided molecules from the two output branches show two almost symmetrical profiles, corresponding to a 50%-50% splitter. When $\Delta U = +6$ kV, the majority of the guided

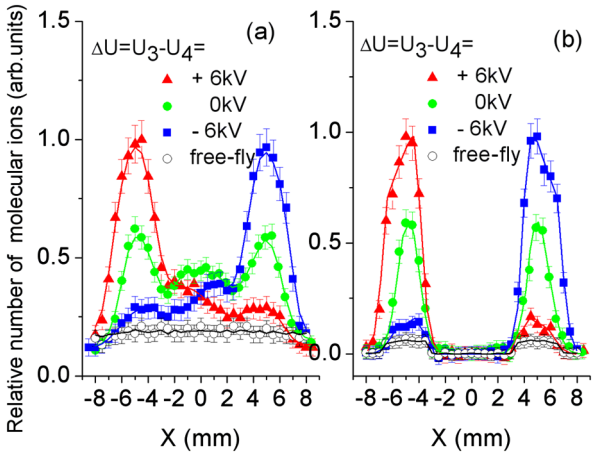

FIG. 2 (color online). Transverse profiles of the guided ND_3 molecular ion signals measured at the two outlets of the EMBS for three selected values of $\Delta U = U_3 - U_4 = +6$ kV (i.e., $U_3 = 16$ kV, $U_4 = 10$ kV, triangles), 0 kV (i.e., $U_3 = 16$ kV, $U_4 = 16$ kV, circles), and −6 kV (i.e., $U_3 = 16$ kV, $U_4 = 10$ kV, squares), respectively. (a) Without the sampling board, (b) with the sampling board. Open symbols correspond to measured ion signals for free-flying molecules without any voltage applied. Solid lines represent the corresponding simulated transverse profiles of guided molecules.

molecules appear in the left branch, while when $\Delta U = -6$ kV, the majority of the guided molecules appear in the right branch. This shows that the ratio of the guided molecular numbers in the two output branches can be efficiently adjusted by changing the voltage difference ΔU.

We simulated the trajectories of ND_3 molecules going through the EMBS by using the 3D classical Monte Carlo method. Because of dc Stark effect, a moving ND_3 molecule in the WFS state $|J = 1, KM = -1\rangle$ in the external electric field experiences a Stark shift in the approximate form $W_E(r) = \{(W_{\text{inv}}/2)^2 + [\mu_e E(r)/2]^2\}^{1/2} - W_{\text{inv}}/2$ [here W_{inv} is the inversion splitting (~ 0.05 cm^{-1}), μ is the magnitude of the dipole moment (1.48 D) and $E(r)$ is the spatial distribution of the electrostatic field], and an electric dipole gradient force is given by $\mathbf{F}(r) = -\nabla W_E(r) = -\mu_e \nabla E(r)$. The simulated ND_3 molecular beam in the state $|J = 1, KM = -1\rangle$ is centered around 300 m/s with a velocity spread of 60 m/s in the longitudinal direction, and has a velocity spread of 15 m/s centered around zero in the transverse direction, and the total number of the simulated molecules is 10^6. The electrostatic-field distribution inside our EMBS is numerically calculated by MAXWELL software. After passing the two sample holes, the simulated molecules arrive at the detection zone, and those molecules within the laser spot at the specified time interval are ionized with an efficiency of 100% and statistically counted. With the transverse moving of the laser spot step by step, a simulated transverse profile for guided molecules is obtained. Solid lines in Fig. 2 show the simulated transverse profiles of guided molecules for three cases. The highest peak of the simulation data is normalized to that of its corresponding experimental results. It is clear from Fig. 2 that our simulated results are in good agreement with our experimental ones, and they have the same asymmetric transverse profile. This shows that the guided molecular number in each output branch is proportional to the integrated area under the corresponding transverse distribution.

Based on the transverse profiles of guided molecules we can study the dependence of the splitting ratio R of our EMBS on the voltage difference ΔU. Here the splitting ratio R is defined as the ratio of the integrated area under the transverse profile of each molecular branch to the total area of the two molecular branches. Solid squares with an error bar and open ones in Fig. 3(a) are the experimental and simulated results, respectively. As we can see from Fig. 3(a), with the change of ΔU from -6 kV to $+6$ kV, the splitting ratio R of the left molecular branch is increased from 10% to 90%, while that of the right branch is reduced from 90% to 10%. When $\Delta U = 0$ kV, a splitting ratio of $R = 50\%$-50% is obtained.

We also studied the dependence of the relative guiding efficiency of molecules on the voltage difference ΔU, and the experimental (see the left ordinate) and simulated (see the right ordinate) results are shown in Fig. 3(b). Here the relative guiding efficiency η of the splitter is defined as the ratio of the total integrated area under the transverse profiles of the two output molecular branches to the total area for the case of $\Delta U = +6$ kV. We can see from Fig. 3(b) that the experimental relative guiding efficiency (solid squares with an error bar) is equal to the simulated absolute guiding efficiency multiplied by 2 (open squares). That is, when $\Delta U = +6$ kV, our absolute guiding efficiency in the experiment can be estimated as $\sim 50\%$. Figure 3(b) shows that with the change of ΔU from -6 kV to $+6$ kV, the absolute guiding efficiency is first reduced from $\sim 50\%$ to $\sim 35\%$, and then increased to 50% again. This "dent" in the profile of η vs ΔU can be explained as follows: the electric dipole interaction experienced by a polar molecule is proportional to the gradient of the electric filed strength and depends on its position inside the EMBS. Because of high longitudinal velocities some molecules with very low transverse velocities near the center of the beam cannot accumulate enough transverse "pushing" effect when passing through the splitting region, they fail to enter one of the two output electrostatic guiding tubes, and directly penetrate the Y-shaped Stark potential barrier and hit the central zone of the sampling board along the beam axis. This occurs severely in the case of $\Delta U = 0$ kV, corresponding to a 50%-50% splitter, since the transverse distribution of the electrostatic field in the splitting region is symmetric about the beam axis, and a zero electric field gradient occurs near the center of the beam axis. With the increase of $|\Delta U|$, the symmetry of the electrostatic-field distribution fades out, and an increasingly larger electric field gradient appears in the center of the beam axis; thus, the molecular loss from the center region of the beam axis is decreased, and the relative guiding efficiency η is increased.

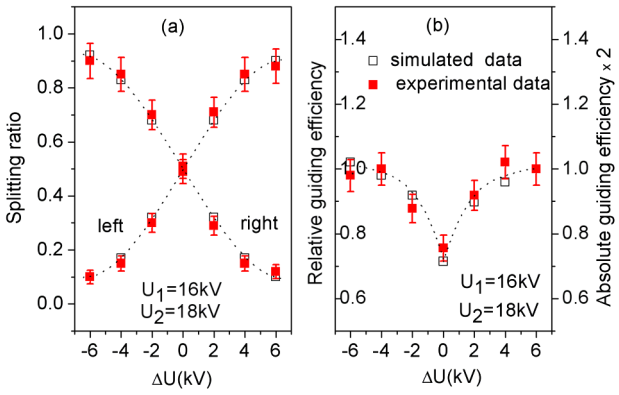

FIG. 3 (color online). Dependences of (a) the splitting ratio R of the EMBS and (b) its relative guiding efficiency η on the voltage difference $\Delta U = U_3 - U_4$ with $U_1 = 16$ kV and $U_2 = 18$ kV. The solid and open squares represent the experimental and simulated results, respectively. The left vertical ordinate in (b) corresponds to the experimental relative guiding efficiency, the right vertical ordinate in (b) corresponds to the simulated absolute guiding efficiency (multiplied by 2). The dotted lines are guides for the eye.

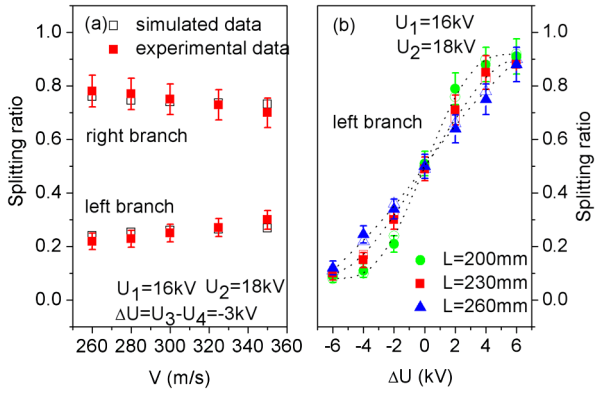

FIG. 4 (color online). The influences of (a) the molecular longitudinal velocity v and (b) the cutting position L on the splitting ratio R. Solid symbols and open symbols correspond to the experimental and simulated results, respectively.

Afterwards, we investigated the dependence of the splitting ratio R of our EMBS on the longitudinal velocity v of the guided molecules when $U_1 = 16$ kV, $U_2 = 18$ kV, and $\Delta U = -3$ kV, and the experimental (solid squares with an error bar) and simulated (hollow squares) results are shown in Fig. 4(a). When the longitudinal velocity of molecules is changed from 260 m/s to 350 m/s, the splitting ratio R of the left branch is increased almost linearly from about 22% to 30%, and R of the right branch is reduced from about 78% to 70%. This is because with the increase of the longitudinal velocity, the molecules spend less time in the splitting region and their trajectories are less affected by the splitting potential field; thus, the difference of the splitting ratio becomes smaller.

Finally, we studied the influence of the cutting position L on the splitting ratio R when $L = 200$, 230, and 260 mm, respectively, and the experimental results are shown in Fig. 4(b). The open symbols represent the simulated results and the solid symbols with an error bar correspond to the experimental results. Figure 4(b) clearly shows that when the cutting position moves closer to the diverging point, the splitting ratio R becomes more sensitive to the voltage difference ΔU. For instance, when $\Delta U = 2$ kV, $L = 200$, 230, and 260 mm, the splitting ratios R of the left branch are about 79%, 71%, and 64%, respectively. However, As $|\Delta U|$ approaches ± 6 kV, the maximal and minimal splitting ratios R of 90% and 10% for the left branch are reached for $L = 200$, 230, and 260 mm, respectively. Therefore, the splitting ratios R of our splitter depends on not only the voltage difference ΔU and the molecular longitudinal velocity v but also the cutting position L.

In conclusion, we have demonstrated our EMBS scheme to split a supersonic ND_3 molecular beam by using a single charged Y wire. The splitting ratio R of our EMBS can be controlled conveniently and efficiently by adjusting the voltage difference ΔU. When $|\Delta U|$ is changed from 0 kV to +6 kV, the splitting ratios are varied from (50%-50%) to (10%–90%). The relative guiding efficiency of our EMBS increases gradually with the increase of $|\Delta U|$ first, and then gets saturated as $|\Delta U|$ approaches +6 kV. The maximal absolute guiding efficiency of ~50% is reached for $\Delta U = +6$ kV. Furthermore, with the increase of the molecular longitudinal velocity, the splitting effect of our EMBS becomes poor, and when the cutting position moves closer to the diverging point, the splitting ratio R becomes more sensitive to the voltage difference ΔU. Such an incoherent molecular-beam splitter, similar to those incoherent atomic-beam splitters using laser or magnetic guiding technique [12–14], can be used to load a double-well electrostatic surface trap (or to load a 2D electrostatic lattice), to perform various experiments using two molecular beams, even to study cold molecular collisions or cold chemistry, etc. Our EMBS scheme can also be miniaturized and integrated on the surface of a chip, and when an ultracold molecular beam, even a coherent molecular Bose-Einstein condensate, is used to realize a single-mode coherent waveguide, a coherent molecular-beam splitter can be formed. Such a coherent EMBS should have some important applications in the field of cold molecular physics, integrated molecule optics, and precise measurement, etc.

This work is supported by the National Nature Science Foundation of China under Grants No. 10674047, No. 10804031, No. 10904037, No. 10974055, and No. 11034002, the National Key Basic Research and Development Program of China under Grants No. 2006CB921604 and No. 2011CB921602, the Basic Key Program of Shanghai Municipality under Grant No. 07JC14017, and the Shanghai Leading Academic Discipline Project under Grant No. B408.

*Corresponding author.
jpyin@phy.ecnu.edu.cn

[1] David W. Keith *et al.*, Phys. Rev. Lett. **66**, 2693 (1991).
[2] Ernst M. Rasel *et al.*, Phys. Rev. Lett. **75**, 2633 (1995).
[3] David M. Giltner *et al.*, Phys. Rev. Lett. **75**, 2638 (1995).
[4] Ch. J. Borde, Phys. Lett. A **140**, 10 (1989).
[5] T. Pfau *et al.*, Phys. Rev. Lett. **71**, 3427 (1993).
[6] J. Baudon *et al.*, J. Phys. B **32**, R173 (1999).
[7] B. Brezger *et al.*, Phys. Rev. Lett. **88**, 100401 (2002).
[8] T. L. Gustavson *et al.*, Phys. Rev. Lett. **78**, 2046 (1997).
[9] M. Kohl *et al.*, Phys. Rev. Lett. **87**, 160404 (2001).
[10] F. Minardi *et al.*, Phys. Rev. Lett. **87**, 170401 (2001).
[11] S. Fray *et al.*, Phys. Rev. Lett. **93**, 240404 (2004).
[12] D. Cassettari *et al.*, Phys. Rev. Lett. **85**, 5483 (2000).
[13] O. Houde *et al.*, Phys. Rev. Lett. **85**, 5543 (2000).
[14] R. Dumke *et al.*, Phys. Rev. Lett. **89**, 220402 (2002).
[15] L. Deng and J. Yin, Opt. Lett. **32**, 1695 (2007).